 doi:10.20944/preprints202203.0393.v1

Article

Twisted Few-Mode Optical Fiber with Improved Height of Quasi-Step Refractive Index Profile

Anton V. Bourdine [1,2,3,4], Vladimir V. Demidov [2], Artem A. Kuznetsov [5*], Alexander A. Vasilets [5,6], Egishe V. Ter-Nersesyants [2], Alexander V. Khokhlov [2], Alexandra S. Matrosova [2,7], Grigori A. Pchelkin [2,8], Michael V. Dashkov [1], Elena S. Zaitseva [1], Azat R. Gizatulin [9], Ivan K. Meshkov [9], Airat Zh. Sakhabutdinov [5], Eugeniy V. Dmitriev [10], Oleg G. Morozov [5], Vladimir A. Burdin [1], Konstantin V. Dukelskii [2,4,7], Yaseera Ismail [11], Francesco Petruccione [11,12], Ghanshyam Singh[13], Manish Tiwari [13], and Juan Yin [14]

1 Department of Communication Lines, Povolzhskiy State University of Telecommunications and Informatics, 23, Lev Tolstoy street, Samara 443010, Russia; bourdine@yandex.ru (A.V.B), burdin@psati.ru (V.A.B.), mvd.srttc@gmail.com (M.V.D.), zaytzewa@inbox.ru (E.S.Z.)
2 JSC "Scientific Production Association State Optical Institute Named after Vavilov S.I.", 36/1, Babushkin street, St. Petersburg 192171, Russia; demidov@goi.ru (V.V.D.), kdukel@mail.ru (K.V.D.), a.pasishnik@gmail.com (A.S.M), khokhlov@goi.ru (A.V.Kh.), ter@goi.ru (E.V.T-N.), beegrig@mail.ru (G.A.P.)
3 "OptoFiber Lab" LLC, Skolkovo Innovation Center, 7, Nobel street, Skolkovo Innovation Center, Moscow 143026, Russia
4 Department of Photonics and Communication Links, Saint Petersburg State University of Telecommunications named after M.A. Bonch-Bruevich, 22, Bolshevikov avenue, St. Petersburg 193232, Russia
5 Department of Radiophotonics and Microwave Technologies, Kazan National Research State University named after A.N. Tupolev-KAI, 10, Karl Marx street, Kazan, 420111, Russia; a.vasilets@mail.ru (A.A.V.) microoil@mail.ru (O.G.M.), azhsakhabutdinov@kai.ru (A.Zh.S.)
6 Faculty of management and engineering business, Kazan Innovative University named after V.G. Timiryasov (IEML), 42, Moskovskaya str., Kazan 420111, Russia;
7 Faculty of Photonics and Optical Information, School of Photonics, ITMO University, bldg. A, 49, Kronverksky alley, St. Petersburg 197101, Russia
8 Institute of Physics, Nanotechnology and Telecommunications, Peter the Great St. Petersburg Polytechnic University, bldg.. II, 29, Politekhnicheskaya str., St. Petersburg 194064, Russia
9 Department of Telecommunication Systems, Ufa State Aviation Technical University, K. Marxa street, 450000 Ufa, Russia; azat_poincare@mail.ru (A.R.G.); mik.ivan@bk.ru (I.K.M.);
10 Department of Quantum Communication Systems Research, Radio Research and Development Institute, Kazakova street, 16, Moscow 105064, Russia; dmitriev@niir.ru (E.V.D);
11 Quantum Research Group, School of Chemistry and Physics, University of KwaZulu-Natal, Durban, 4001, South Africa; ismaily@ukzn.ac.za (Y.I.), petruccione@ukzn.ac.za (F.P.)
12 National Institute for Theoretical Physics, KwaZulu-Natal, South Africa
13 Department of Electronics and Communication Engineering, School of Electrical and Electronics & Communication Engineering, Manipal University Jaipur, J.L.N Road, Jaipur 302017, Rajasthan, India; gsingh.ece@mnit.ac.in (G.S.), manish.tiwari@jaipur.manipal.edu (M.T.)
14 Division of Quantum Physics and Quantum Information, University of Science and Technology of China, No.99 Xiupu Road, Pudong District, Shanghai, China; yinjuan@ustc.edu.cn (J.Y.)
* Correspondence: artem.a.kuznetsov@bk.ru; Tel.: +79196425689

Abstract: This work presents designed and fabricated silica few-mode optical fiber (FMF) with induced twisting 10 and 66 revolutions per meter, core diameter 11 μm, typical "telecommunication" cladding diameter 125 μm, improved height of quasi-step refractive index profile and numerical aperture 0.22. Proposed FMF supports 4 guided modes over "C"-band. We discussed selection of specified optical fiber parameters to provide desired limited mode number over mentioned wavelength range. Some results of tests, performed with pilot samples of manufactured FMF, are represented, including experimentally measured spectral responses of laser-excited optical signals, that comprise researches and analysis of few-mode effects, occurring after fiber Bragg grating writing.

Keywords: twisted optical fiber; chirality; laser beam profile; differential mode delay; laser-based few-mode optical signal transmission; fiber Bragg grating; few-mode effects

 doi:10.20944/preprints202203.0393.v1

1. Introduction

Twisted optical fibers are known since the early of 1980s: here the concept of fiber spinning was the first time originally introduced in the work [1]. The fabrication technique of twisted optical fibers is based on rotation of preform during the fiber drawing [1] or directly spinning of the drawn optical fiber [2]. Twisted singlemode optical fibers are usually considered as fibers with reduced polarization mode dispersion (PMD) [1-4], while induced chirality (including twisting) over multimode optical fibers is declared as the method for differential mode delay (DMD) decreasing with total bandwidth improvement [5, 6].

Nowadays, chiral optical fibers (both with typical coaxial geometry (core, bounded by intermediate and/or outer solid cladding) and microstructured/photonic crystal optical fibers) are considered as alternative unique fiber optic elements with great potentiality for various applications in fiber optic sensors [7–10].

At the same time, many recently published works demonstrated new effects, occurring in fiber Bragg gratings (FBGs), written in FMFs as well as in multimode optical fibers (MMFs), under laser-source excitation. A lot of many recently published works demonstrated few-mode operation of these conventional, tilted or slanted FBGs on MMFs and FMFs in vibration, temperature, deformation, displacement, bending etc. fiber optic sensors [11–20].

A few-mode regime adds a new another one dimension to the space of parameters: it is associated with guided modes of particular order, which limited number (from two to a few dozens) transfer the most part of optical signal power over tested optical fiber. We suppose, that twisted FMF with recorded FBG can be considered as new complicated fiber optic element with unique features and great potentiality for application in fiber optic sensors.

This work is focused on design and fabrication of chiral few-mode optical fiber (FMF) with specified limited (3...4) guided modes, supporting over “C”-band. Therefore, at the first stage, by using commercially available software with rigorous numerical finite element method, technological / geometrical parameters were specified to provide desired few-mode regime operation of designed FMF.

We described performed adaptation of the conventional technique for drawing optical fibers to fabricate designed FMF with induced twisting under small as well as large number of revolutions per meter. Some results of theoretical and experimental researches, performed for pilot samples of manufactured FMF, are represented, including experimentally measured spectral responses of laser-excited optical signals, that comprise researches and analysis of few-mode effects, occurring after fiber Bragg grating recording.

2. Design of FMF: selection of geometrical parameters to provide desired limited number of guided modes

At the first stage, we utilized rigorous numerical finite element method, used in COMSOL Multiphysics software, to analyze preliminary designed set of specified step-index optical fibers with the same typical “telecommunication” cladding diameter 125 μm, but differing by combination of core diameter and numerical aperture (e.g. height of refractive index profile). Here for each designed optical fiber sample, guided modes (which satisfy to the cut-off condition) were defined, and their effective refractive indexes were computed. The main criterion was focused on providing of limited (3…4) transversal guided modes propagation over FMF under laser source excitation at the wavelength λ=1550 nm.

We performed analysis of FMF by earlier on developed and successfully verified method [21-23], based numerical solution of linear Maxwell equation system, written for a homogeneous isotropic dielectric in the absence of free charges and currents and reduced to wave equations for the vectors of electric (E) and magnetic (B) fields [24]:

Preprints (www.preprints.org) | NOT PEER-REVIEWED | Posted: 30 March 2022 doi:10.20944/preprints202203.0393.v1

$$\nabla \times \left(\frac{1}{\mu}\nabla \times E\right) - k_0^2 \varepsilon E = 0, \quad (1)$$

where k_0 is wave number ($k_0 = 2\pi/\lambda$); ε is the dielectric permeability ($\varepsilon = n^2$, n is refractive index); μ is magnetic permeability.

By taking into account satisfaction to the perfectly matched layer (PML) conditions, equation (1) was transformed to the following form [25]:

$$\nabla \times \left(\frac{1}{\mu'}\nabla \times \frac{1}{[S]}E\right) - k_0^2 \varepsilon' \frac{1}{[S]}E = 0, \quad (2)$$

where ε' и μ' are modified dielectric and magnetic permeability; [S] is matrix of PML layer coefficients.

Solution of equation (2) is equation of electromagnetic wave, propagating along z-axis of optical fiber [24]:

$$E(z,t) = E_0 \exp\left[j\left(\omega t - \frac{\omega}{c} n_{\text{eff}} z\right)\right], \quad (3)$$

where E_0 is amplitude of electric field strength; ω is circular frequency; c is light speed in vacuum; t is time.

Effective refractive index n_{eff} is defined by numerical solution of equation (3), and related transversal mode is identified (in terms of linear polarized modes LP_{lm} – e.g. azimuthal and radial orders l and m) by comparison computed radial mode field distribution with pre-defined field patterns of known order modes LP_{lm}, which are exact solutions for scalar wave equation, written for model optical fiber with ideal step index or unbounded parabolic refractive index profiles, and described by Bessel or Laguerre-Gaussian functions [26, 27].

Table 1 shows results of optical fiber analysis, performed by a rigorous finite element numerical method in COMSOL Multiphysics software under wavelength $\lambda = 1550$ nm. We considered ideal step-index refractive index profile, the same cladding diameter 125 μm (that corresponds to conventional telecommunication optical fibers), three various core diameters (8.3, 10.0, and 11.0 μm) and six values of numerical aperture NA (0.14, 0.16, 0.18, 0.20, 0.22, and 0.24 – it corresponds to approximately the difference between core and cladding refractive indexes 0.02). We start from the core diameter 8.3 μm as the typical value for standard single mode optical fibers (SMFs) of ITU-T Rec. G.652 [28]. It was supposed, that even the weak improvement of refractive index profile height, in comparison with ratified SMF, may provide desired few-mode regime with 3…4 transversal guided mode propagation at $\lambda = 1550$ nm. However, results of computation shew, that following increasing both core diameter and numerical aperture (e.g. refractive index profile height is required).

Table 1. Results of optical fiber analysis, performed my rigorous numerical method: step-index optical fibers under various combinations of core diameter and numerical aperture ($\lambda = 1550$ nm)

№	Core diameter, μm	Cladding diameter, μm	Numerical aperture *NA*	Mode composition	n_{eff}	Δn_{eff}
1	8.3	125	0.14	LP_{01}	1.460478	–
2	8.3	125	0.16	LP_{01}	1.462210	
				LP_{11}	1.457688	0.004522
3	8.3	125	0.18	LP_{01}	1.464263	
				LP_{11}	1.459082	0.005181
4	8.3	125	0.20	LP_{01}	1.466624	
				LP_{11}	1.460940	0.005684
5	8.3	125	0.22	LP_{01}	1.469284	
				LP_{11}	1.463199	0.006085
6	8.3	125	0.24	LP_{01}	1.472237	

Preprints (www.preprints.org) | NOT PEER-REVIEWED | Posted: 30 March 2022 doi:10.20944/preprints202203.0393.v1

				LP_{11}	1.465821	0.006416
				LP_{21}	1.458136	0.014101
				LP_{02}	1.457159	0.015078
7	10	125	0.14	LP_{01}	1.461181	
				LP_{11}	1.457847	0.003334
8	10	125	0.16	LP_{01}	1.463027	
				LP_{11}	1.459219	0.003808
9	10	125	0.18	LP_{01}	1.465177	
				LP_{11}	1.461012	0.004165
10	10	125	0.20	LP_{01}	1.467622	
				LP_{11}	1.463176	0.004446
				LP_{21}	1.457854	0.009768
				LP_{02}	1.457139	0.010483
11	10	125	0.22	LP_{01}	1.470355	
				LP_{11}	1.465682	0.004673
				LP_{21}	1.459875	0.010480
				LP_{02}	1.458498	0.011857
12	10	125	0.24	LP_{01}	1.473371	
				LP_{11}	1.468510	0.004861
				LP_{21}	1.462343	0.011028
				LP_{02}	1.460621	0.012750
13	11	125	0.14	LP_{01}	1.461499	
				LP_{11}	1.458455	0.003044
14	11	125	0.16	LP_{01}	1.463387	
				LP_{11}	1.459994	0.003393
15	11	125	0.18	LP_{01}	1.465572	
				LP_{11}	1.461914	0.003658
				LP_{21}	1.457563	0.008009
				LP_{02}	1.457061	0.008511
16	11	125	0.20	LP_{01}	1.468048	
				LP_{11}	1.464179	0.003869
				LP_{21}	1.459378	0.008670
				LP_{02}	1.458241	0.009807
17	11	125	0.22	LP_{01}	1.470808	
				LP_{11}	1.466767	0.004041
				LP_{21}	1.461642	0.009166
				LP_{02}	1.460198	0.010610
18	11	125	0.24	LP_{01}	1.473847	
				LP_{11}	1.469664	0.004183
				LP_{21}	1.464288	0.009559
				LP_{02}	1.462650	0.011197
				LP_{31}	1.458078	0.015769

For example, combination of the SMF "nominal" core diameter 8.3 μm and maximal (from the researched range) numerical aperture value NA=0.24 provides technical satisfaction of the cut-off condition for desired 4 modes – the fundamental LP_{01} and higher order modes LP_{02}, LP_{11}, LP_{21}. However, the last two modes LP_{02} and LP_{21} are unacceptably instable to propagation over long distances due to their field concentration in the cladding: here, optical confinement factor P_{co} (e.g., mode power, transferred over core) for both mentioned above modes is inadmissible low (P_{co}<0.5). Therefore, we conclude, that none of researched combinations of core diameter 8.3 μm and 6 tested numerical aperture values NA=0.14…0.24 do not provide desired 4-mode operation at wavelength λ=1550 nm.

 doi:10.20944/preprints202203.0393.v1

The same matter corresponds to core diameter 10.0 μm and *NA*=0.20: here also higher-order modes LP_{02} and LP_{21} satisfy cutoff condition under unacceptable low optical confinement factor P_{co}<0.5, while desired 4-mode operation is achieved for numerical aperture range *NA*=0.22…0.24. Following improvement of core diameter up to 11 μm shew the best results for *NA*=0.20 and *NA*=0.22: all 4 modes satisfy to the cutoff condition under required optical confinement factor P_{co}>0.5. Lower *NA*=0.18 led to inappropriate low P_{co}<0.5 for the same last two higher-order modes, while increased *NA*=0.24 provides satisfaction of the cutoff condition for 5th mode LP_{31}.

Therefore, according to computation results, we selected following configuration for fabricated FMF: core diameter 11 μm, typical "telecommunication" cladding diameter 125 μm, numerical aperture *NA*=0.22.

3. Pilot FMF 11/125 with improved height of quasi-step refractive index profile and induced chirality

According to defined above technological parameters, a preform of the desired FMF 11/125 with the numerical aperture *NA*=0.22 was prepared by conventional modified chemical vapor deposition (MCVD) method [29]. Fig.1 presents measured refractive index profile with improved height of FMF fabricated preform.

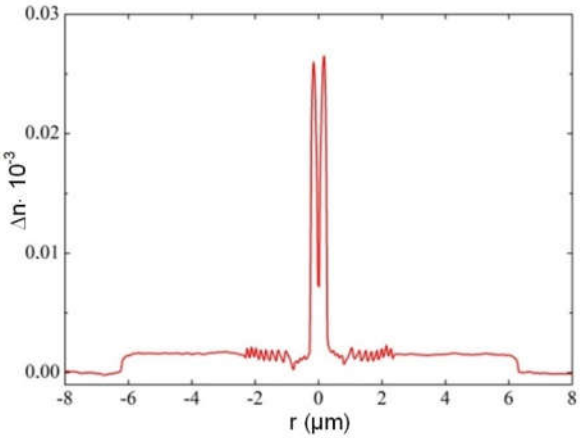

Figure 1. Refractive index profile of pilot FMF preform (measured by refractometer Photon Kinetics P101)

The general form of fabricated preform refractive index profile is quasi-step. Moreover, there is a dip of refractive index in the core center, that is typical for MCVD technique: it is caused by highly volatile GeO_2 dopant diffusion during support tube collapse. Here the absolute height of the profile reaches ~0.27, while dip is ~0.08. As a result, to correctly evaluate refractive index profile height, we computed the area of central (core) part and further estimated the effective height of the profile. For researched prepared FMF 11/125 preform, this parameter was ~0.018, that is equivalent to numerical aperture *NA*=0.22.

We performed some modifications of the drawing tower to induce twisting on FMF during its drawing. The detailed description of modification is represented in the earlier on published work [30]. Usually, preform is fixed in a mechanical chuck of the feed unit, that input preform to the heat space of high temperature furnace. Preform is kept in a stationary position and redrawn without rotation. To induce desired chirality over manufactured FMF, we integrated the stepper motor to the feed unit, which continuously rotates preform under the set speed and adds a new rotation function to the drawing system. The maximal rotation speed of the stepper motor is 200 rpm, which provides chirality of approximately 100 revolutions per meter under the drawing speed 2 m per minute. The minimal motor rotation speed is 20 revolutions per meter (rpm), while the maximal is 200 rpm. Therefore, under slow drawing speed 2...3 m/min (that is usually used for

Preprints (www.preprints.org) | NOT PEER-REVIEWED | Posted: 30 March 2022 doi:10.20944/preprints202203.0393.v1

manufacturing special or experimental optical fibers), it induces twisting with 10 and 66 rpm, respectively.

Fig. 2 shows image of the end-face of fabricated pilot sample of chiral FMF 11/125 with numerical aperture *NA*=0.22, drawn from described above manufactured preform. Fig. 3 presents near field laser beam profile (operating wavelength λ=1550 nm) after propagation over the fabricated FMF 11/125 by CCD camera.

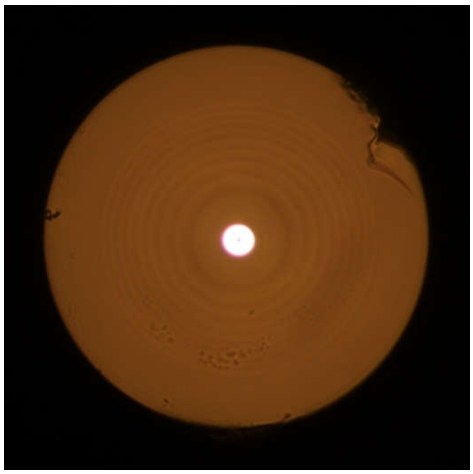

Figure 2. Image of the end-face of fabricated pilot 4-mode FMF 11/125 with numerical aperture *NA*=0.22 (high-resolution optical microscope Nikon Eclipse N-U)

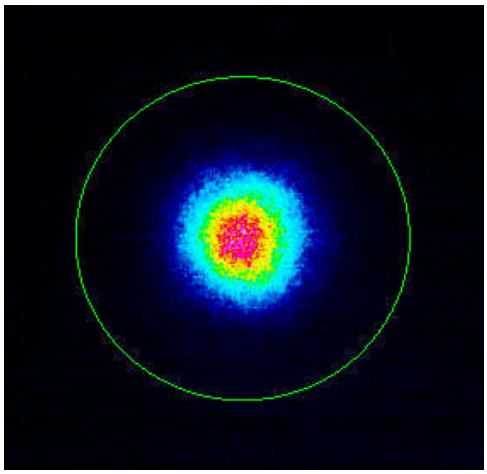

Figure 3. Near field laser beam profile (operating wavelength λ=1550 nm), measured after propagation over pilot sample of FMF 11/125 by CCD camera DataRay WinCamD-LCM-C-TE

We measured both 10 rpm and 66 rpm pilot sample 50 m length FMF 11/125 attenuation $\alpha(\lambda)$ by cutback method over wavelength band λ = 900–1700 nm by using a 64642 HLX halogen lamp (OSRAM) as a light source, programmable monochromator (ANDO), germanium photodiode (wavelength range 900...1700 nm), optical amplifier (eLockIn), and optical power meter (and ANDO AQ-1135E).

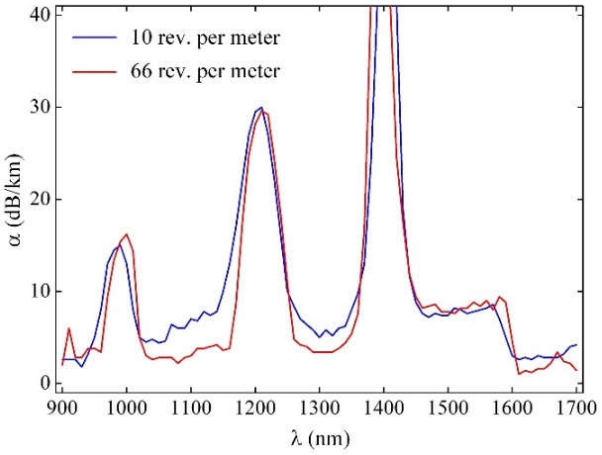

Figure 4. Attenuation of manufactured 50 m length FMF 11/125 samples with induced chirality 10 and 66 rpm

Measured attenuation curves $\alpha(\lambda)$ contain typical resonance "water" peaks with strong loss due to simplified and rapid technique for FMF preform fabrication without hydroxyl (OH^-) dopants extraction: here we just focused on chiral FMF pilot sample length manufacturing with specified geometry parameters, that should provide desired

Preprints (www.preprints.org) | NOT PEER-REVIEWED | Posted: 30 March 2022 doi:10.20944/preprints202203.0393.v1

few-mode operation by low widening core diameter and strong improvement of refractive profile height, and did not pay attention to attenuation reduction. In the same way, increased attenuation (in comparison with commercially available silica optical fibers [28]) at the central regions of the "C"- and "O"-bands, which reaches almost α=7...8 dB/km, was expected due to intentional excluding (to reduce reagent consumption and also to simplify preform fabrication process) of typical operation of Fluorine (F) doping to the core region, that helps to decrease GeO_2 dopant unwanted influence on attenuation increasing.

Fig. 4 demonstrates, that attenuation curve $\alpha(\lambda)$ over "flat" regions between the resonance peaks for FMF with twisting 66 rpm is some lower in comparison with chiral FMF 10 rpm. It may be explained by more smoothing of refractive index profile typical MCVD technological defects under more rapid twisting of preform during optical fiber drawing.

4. Dispersion parameters of guided modes, propagating in the pilot sample FMF 11/125 with improved height of quasi-step refractive index profile

During the next stage, we computed spectral characteristics of dispersion parameters of guided modes, satisfying to cut-off condition for fabricated pilot sample of FMF 11/125. For this purpose, it was proposed to utilize earlier on developed simple and fast approximate method, which is a modification of the Gaussian approximation, extended to the case for estimation of the transmission parameters of arbitrary order modes, propagating in a weakly guiding optical fiber with an arbitrary axially symmetric refractive index profile [31] with following optionally (in appropriate case) accuracy improvement by rigorous numerical method of mixed finite elements [32]. This extended modification of the Gaussian approximation (EMGA) is based on combination of the stratification method [26] and "classical" Gauss approximation [27]. Stratification method provides ability to represent complicated form of researched optical fiber refractive index profile with high detailing and corresponding technological defects (including local refractive index fluctuations), in spite of the most approximate methods, which typically utilize one or set of smooth functions. Proposed approach significantly reduces computational error during direct calculation of transmission parameters of guided modes in optical fiber with large core diameter (in comparison with singlemode optical fibers) and complicated form of refractive index profile [31, 32]. Here only one variational parameter – normalized mode field radius R_0 – should be determined as a result of characteristic equation solution, while R_0 within the "classical" Gaussian approximation is basis, and it completely defines all desired guided mode transmission parameters. According to Gaussian approximation, radial mode field distribution is represented by well-known approximating expression, based on Laguerre-Gaussian functions [27], that corresponds to exact solution of scalar wave equation, written for weakly guiding optical fiber with an ideal inbounded parabolic refractive index profile. This permits to derive and write analytical expressions for variational expression and characteristic equation in the form of finite nested sums, and further their first and second derivations – mode delay and chromatic dispersion parameter. Therefore, developed approximate method EMGA does not require high computational resources (even during higher-order mode dispersion parameter estimation) and provides low (less than 1% [26, 27]) computational error.

Fig. 5 shows an equivalent quasi-step refractive index profile of the analyzed FMF 11/125 with a numerical aperture NA=0.22, restored by report of measurements, performed for drawn optical fiber.

At the first stage, we computed optical confinement factor for modes, propagating in a mentioned above FMF 11/125, over wavelength range λ = 700...1700 nm. The results are presented in the form of a diagram on Fig. 6.

Preprints (www.preprints.org) | NOT PEER-REVIEWED | Posted: 30 March 2022 doi:10.20944/preprints202203.0393.v1

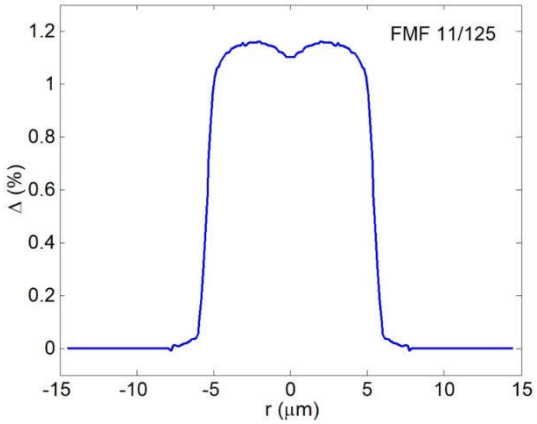

Figure 5. Equivalent quasi-step refractive index profile with improved height, restored by measurement report data

According to computational results, desired 4-mode optical signal transmission is provided by researched FMF 11/125 over band λ = 1450...1700 nm. Generally, 38 LP_{lm} modes with l = 0…7 azimuthal and m=1…9 radial orders nominally satisfy to the cut-off condition at the least researched wavelength range bound λ = 700 nm. However, only for 19 modes with also l = 0…7, but m=1…4 orders optical confinement factor is more P_{co}≥0.5 for the same wavelength.

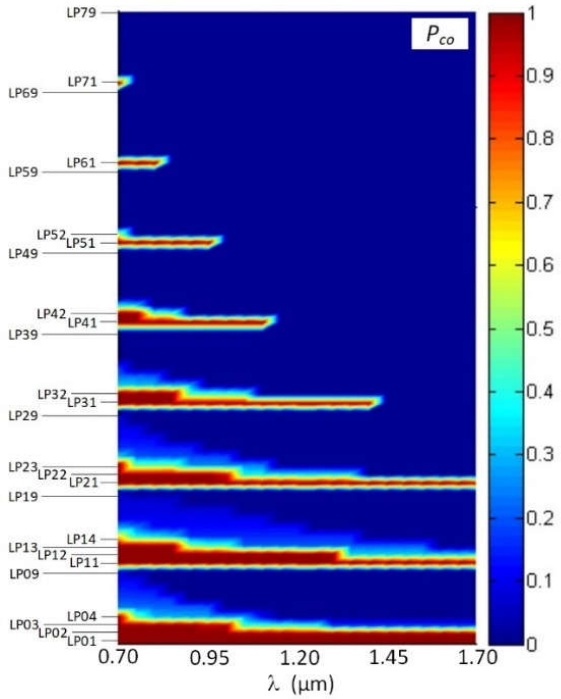

Figure 6. Diagram of the optical confinement factor distribution between modes of FMF 11/125 over the wavelength range λ= 700 ... 1700 nm.

At the central region of the "O"-band (λ = 1300 nm), researched FMF 11/125 supports 6 guided modes, that satisfy the cut-off condition under the optical confinement factor value more P_{co}≥0.5: they are listed in previous Section 2 – LP_{01}, LP_{11}, LP_{21}, LP_{02} modes and two additional higher-order modes LP_{12}, LP_{31}. We computed spectral curves of dispersion parameters for those mentioned above 6 guided modes. Results are represented on Fig. 7(a) spectral characteristics of mode delay and (b) chromatic dispersion coefficient. Analysis of mode delay curves shows, that DMD reaches 18.35 ns/km over λ=1300 nm wavelength region,

Preprints (www.preprints.org) | NOT PEER-REVIEWED | Posted: 30 March 2022 doi:10.20944/preprints202203.0393.v1

while near λ=1550 nm DMD decreases down to 14.93 ns/km due to "suppression" of two higher-order modes LP_{12} and LP_{31}.

By comparing spectral characteristics of the chromatic dispersion coefficient for the fundamental and higher-order modes, computed curves are generally similar to spectral characteristic of chromatic dispersion coefficient for standard telecommunication single-mode optical fiber (SMF) of ITU-T Rec. G.652 [28]. Here zero dispersion wavelength of both the fundamental and higher-order guided modes corresponds to wavelength range λ=1300 ... 1350 nm. Maximal deviation of this parameter D between higher-order guided modes was 27.09 ps/(nm·km) at λ=1300 nm and 4.97 ps/(nm·km) at λ=1550 nm.

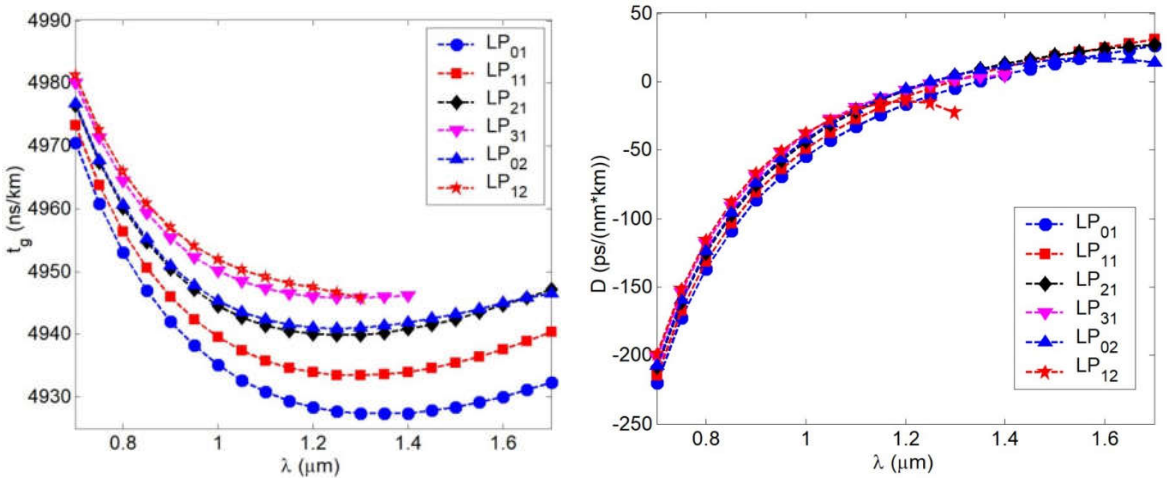

(a) (b)

Figure 7. Spectral characteristics of guided mode dispersion parameters: **(a)** mode delay. **(b)** chromatic dispersion coefficient

5. Experimental research of spectral responses of FBG, written over chiral FMF 11/125 with improved height of quasi-step refractive index profile

Two FBG samples were written on the short (less 1.5 m) segments of SMF (Rec. ITU-T G.652 [28]) and fabricated pilot sample of chiral FMF 11/125 by Lloyd ineterferometric setup workstation under the same mask (with the same grating period), providing expected Bragg wavelength about $\lambda_B \approx 1550$ nm. We performed preliminary measurements of both FBG spectral responses under propagation of optical signal, generated by continuos emission (CE) wideband laser diode (LD) with operating wavelength λ=1550 nm and pigtailed by SMFs. Conventional setup was utilized for FBG spectral response measurement by optical spectrum analyzer (OSA) with fiber optic circulator (CIR), also pigtailed by SMFs. Described above scheme for testing of FBG, written on FMF, is shown on Fig. 8. Both tested FBGs were jointed to SMF pigtail by fusion splicer, and further connected to circulator via corresponding fiber optic adapter.

Results of measurements – OSA software screenshots – are represented on Fig. 9(a) and (b). Comparison of two measured spectral responses show, that detected Bragg wavelength of FBG, written on FMF 11/125, is higher up to 16.46 nm (λ_B =1567.50 nm), than for FBG on SMF (λ_B =1551.04 nm). This suggests, that effective refractive index for the fundamental mode LP_{01} of FMF is some higher, in comparison with the fundamental mode LP_{01} of SMF, in approximately 1%. Spectral response of FBG on FMF contains main and periphery peaks. It may be considered as superposition of several modes, corresponding to transversal mode components, that led to response widening, and confirms desired few-mode regime of FMF operation at the central wavelength of "C"-band (λ=1550 nm).

Preprints (www.preprints.org) | NOT PEER-REVIEWED | Posted: 30 March 2022 doi:10.20944/preprints202203.0393.v1

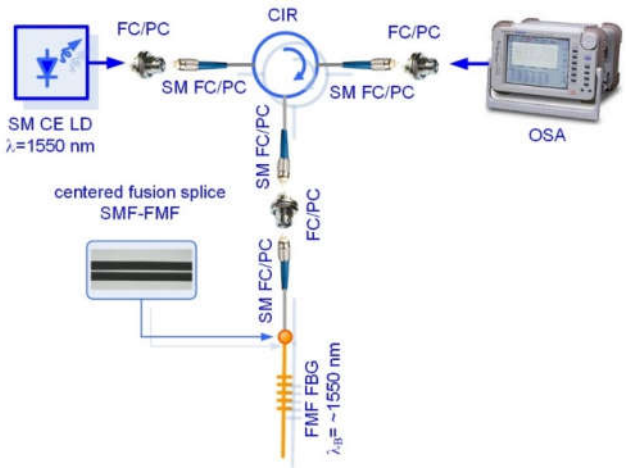

Figure 8. Conventional setup for FBG spectral response measurement: testing of FBG, written on FMF under laser-based few-mode operation.

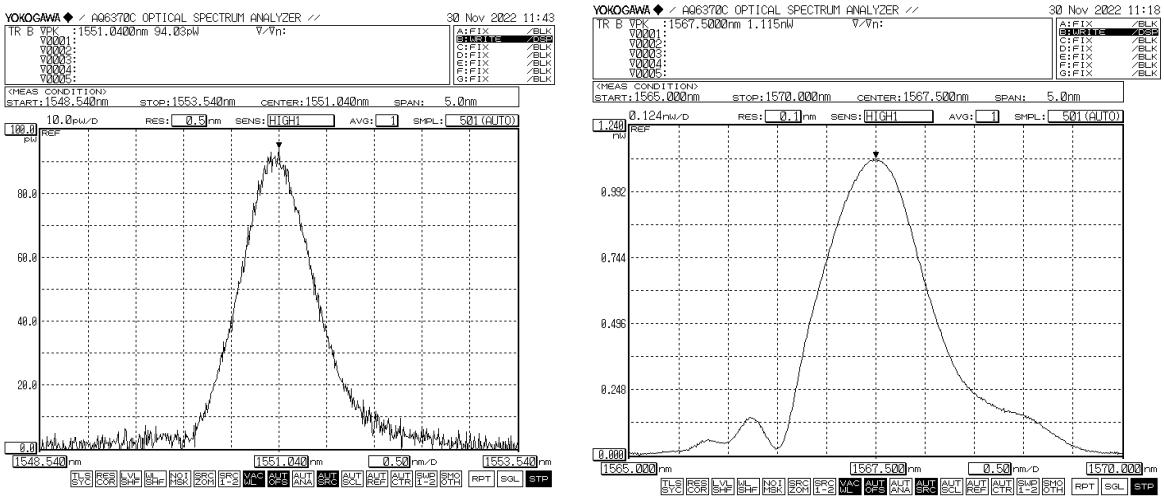

(a) (b)

Figure 9. Spectral responses of FBG, excited by laser-source (CE LD, λ=1550 nm): **(a)** FBG on SMF; **(b)** FBG on FMF 11/125.

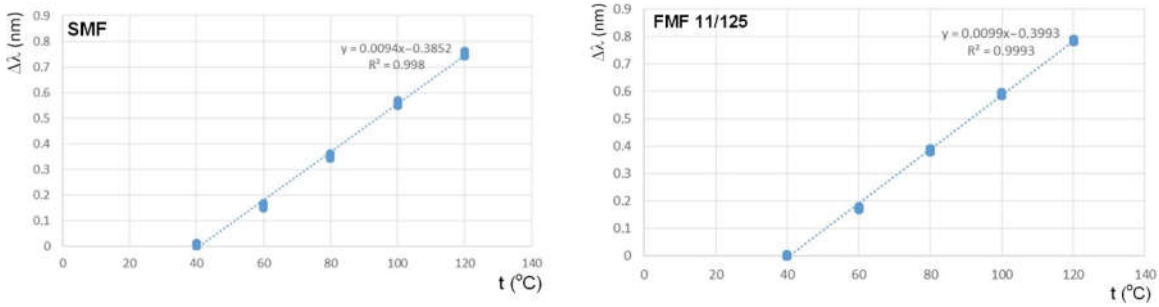

(a) (b)

Figure 10. FBG Bragg wavelength λ_B shifting sensitivity to the temperature action: **(a)** FBG on SMF; **(b)** FBG on FMF 11/125.

Preprints (www.preprints.org) | NOT PEER-REVIEWED | Posted: 30 March 2022 doi:10.20944/preprints202203.0393.v1

The next set of tests was concerned with research of FBG Bragg wavelength λ_B shifting sensitivity to the temperature action with following comparison. We placed sequentially both FBGs to the thermostat and discretely varied temperature from +40°C up to +120°C with a step 20°C. Here Bragg wavelength λ_B under the least bound temperature +40°C was considered as the reference value for the following estimation of λ_B shifting under the temperature increasing. Results are represented on the Fig. 10 in the form of diagrams. Both dependences are highly linear, while the slope for FBG on FMF is some higher (approximately on 5%).

By analogy with the previous measurements, we performed test series, focused on researh and comparison sensitivity of FBGs on SMF and FMF to meachanical action. For these researches, we placed FBGs to the precision translation stage, that provides tensile and following precision particular elongation of researhed optical fiber segment with wrotten FBG over the range 100…250 μm with a step 50 μm. Here Bragg wavelength under the unstrained state was considered as the reference value for the following estimation λ_B shifting $\Delta\lambda$ under the described mechanical action. Results are represented on the Fig. 11 also in the form of diagrams. Both dependences are also highly linear, while the slope for FBG on FMF is some higher (approximately on 2.5%).

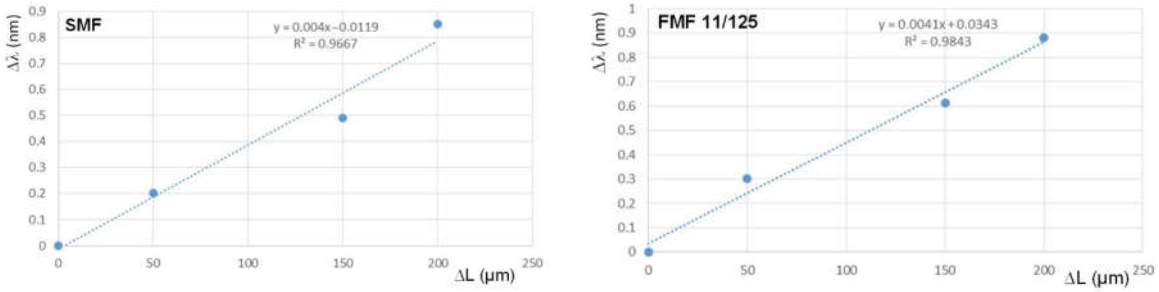

(a) (b)

Figure 11. FBG Bragg wavelength λ_B shifting sensitivity to the mechanical action: **(a)** FBG on SMF; **(b)** FBG on FMF 11/125.

The next test series was concerned with researches of few-mode effects, occurring during laser-excited optical signal propagation over FBG, written in FMF 11/125, under some various stress actions. Here we utilized "direct" FBG spectral response measurement scheme without fiber optic circulator (Fig. 12), and tested sample FBG on FMF was pigtailed by using fusion splicer by short SMF pigtails with length not more 140 mm to avoid conversion of higher-order FMF guided modes to leakage / cladding modes in SMF pigtail [33].

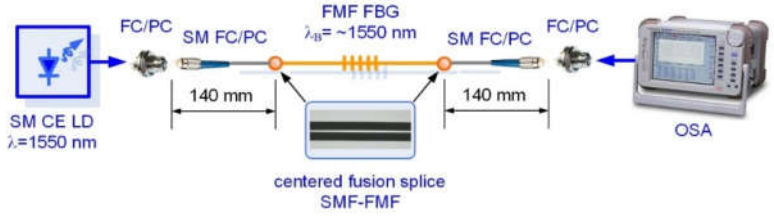

Figure 12. Conventional setup for FBG spectral response measurement: testing of FBG, written on FMF under laser-based few-mode operation

Spectral response, measured for FBG on FMF 11/125 in an unperturbed state (that would be further considered as the reference) is presented on Fig. 13. Here 3 peaks (one the main peak (1567.24 nm), two periphery peaks (1566.65 nm and 1567.96)) could be seen quite distinctly. During the next tests, we measured spectral responses under forming

Preprints (www.preprints.org) | NOT PEER-REVIEWED | Posted: 30 March 2022 doi:10.20944/preprints202203.0393.v1

FMF loop with radius 15 mm before, on and after FBG. Results are shown on Fig. 14. As expected, in all cases Bragg wavelength shifting was detected. However, response smoothing as well as periphery peak dropout were noticed. Here λ_B shift down to $\Delta\lambda$=0.24 nm under loop before and after FBG, while for the loop on FBG λ_B became longer up to 0.08 nm in comparison with the reference response main peak value. Second test series was concerned with spectral response measurements after placing loops with radius 86 and 63 mm over researched segment of FMF 11/125 with written FBG. Results are demonstrated on Fig. 15. Here again response smoothing and periphery peak dropout are noticed under the same Bragg wavelength shifting down to 0.16 and 0.20 nm.

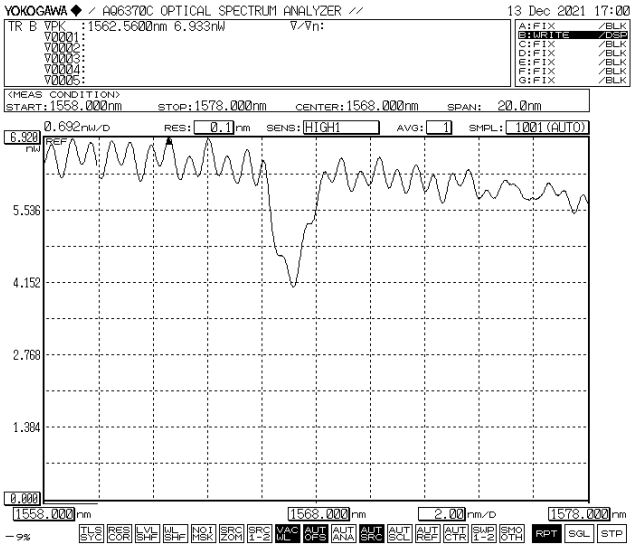

Figure 13. Reference spectral response of unperturbed FBG, written on FMF 11/125

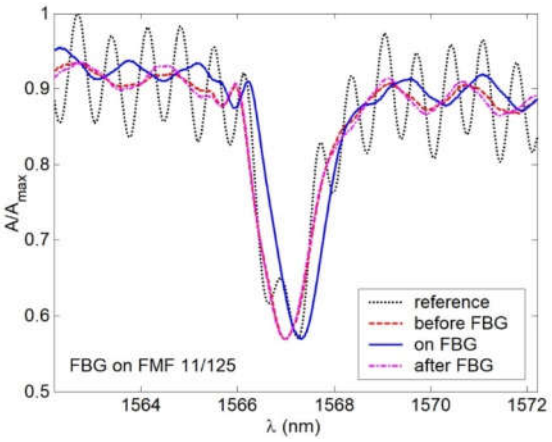

Figure 14. Spectral responses under 15 mm loop before, after and on the FBG, written on FMF 11/125.

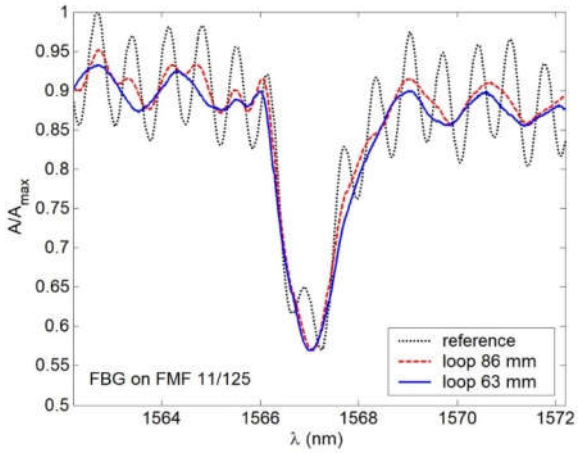

Figure 15. Spectral responses under 86 and 63 mm loops, placed over FMF 11/125 with written FBG.

Conclusion

This work is devoted to the design and fabrication, as well as experimental and theoretical researches of the parameters of chiral FMF 11/125 with an induced twisting and improved height of a quasi-step refractive index profile, that provides 4-mode operation over "C"-band. Based on the series of simulation of described optical fiber, we selected specified technological parameters to support desired 4 guided mode over mentioned

 doi:10.20944/preprints202203.0393.v1

above "C"-band: core diameter 11 μm, cladding diameter 125 μm, and numerical aperture *NA* = 0.22.

Successfully fabricated pilot sample lengths of described above chiral FMF 11/125 with induced twisting of 10 and 66 rpm are presented. Results of measured attenuation shew expected increased loss α=7...8 dB/km over "C"- and "O"-bands, explained by intentionally simplified technique for FMF preform manufacturing by excluding typical F doping to optical fiber preform core region, that helps to decrease GeO_2 dopant unwanted influence on attenuation increasing.

We performed analysis of designed and fabricated FMF 11/125: here data from measurement report were utilized to restore real form of quasi-step refractive index profile. Orders of guided modes, satisfying to the cut-off condition, were defined over researched wavelength band λ=700…1700 nm (4…6 guided modes were localized over "C"- and "O"-band, respectively). Spectral characteristics of dispersion parameters (mode delay and chromatic dispersion coefficient) for defined guided modes were computed for mentioned above researched wavelength range. Analysis of the mode delay curves showed, that at the wavelength λ=1300 nm DMD reaches 18.35 ns/km, while at the wavelength λ=1550 nm, it reduces down to 14.93 ns/km. By comparing spectral characteristics of the chromatic dispersion coefficient for the fundamental and higher-order modes, computed curves are generally similar to spectral characteristic of chromatic dispersion coefficient for conventional SMF (ITU-T Rec. G.652): here zero dispersion wavelength of both the fundamental and higher-order guided modes corresponds to wavelength range λ=1300 ... 1350 nm.

FBG was wrote in the sample of fabricated FMF 11/125 segment, and test series were performed to research a few-mode effects, occurring during laser-excited optical signal propagation over FMF with written FBG both unperturbed and under the temperature or mechanical actions. Main and periphery peaks were localized on the spectral response of unperturbed FMF FBG, while under the stress besides the expected Bragg wavelength shifting, spectral response smoothed and periphery peaks drop out. Results of performed theoretical and experimental researches shew a good potentiality for utilization of designed and fabricated twisted FMF 11/125 in various applications of selected order guided mode management as well as in fiber optic sensors.

Supplementary Materials: Not applicable.

Author Contributions: Conceptualization, A.V.B., V.V.D., G.S., M.T., V.J.; methodology, A.V.B, V.A.B., K.V.D., Y.I., O.G.M., F.P., J.Y.; development of technique for twisted optical fiber fabrication, modification of drawing tower, chiral microstructured optical fiber fabrication, V.V.D, K.V.D., A.V. Kh., A.S.M., G.A.P., E.V.T.; measurements of geometry parameters, laser beam profile, attenuation, V.V.D, A.V. Kh., A.S.M., G.A.P., E.V.T.; writing FBG, measurements of FBG spectral responses, A.V.B., A.Yu.B., M.V.D., A.S.E., A.A.K., A.Zh.S., E.S.Z., A.R.G., I.K.M., E.V.D.; writing—review and editing, A.V.B., .V.D., A.V.V., A.A.K.; visualization, A.V.B., V.V.D., M.V.D., A.A.K., A.A.V., E.V.D., A.R.G., I.K.M.; supervision, A.V.B..; project administration, A.V.B.

Funding: This research was funded by RFBR, DST, NSFC and NRF according to the research project 19-57-80016 BRICS_t.

Institutional Review Board Statement: Not applicable.

Informed Consent Statement: Not applicable.

Conflicts of Interest: The authors declare no conflict of interest.

References

1. Barlow, A.J.; Ramskov-Hansen, J.J.; Payne D.N. Birefringence and polarization mode dispersion in spun single-mode fibers. *Applied Optics*. **1981**, *20*, 2962–2968.
2. Hart. A.C. Jr.; Huff, R.G.; Walker, K.L. Method of making a fiber having low polarization mode dispersion due to a permanent spin. *U.S. Patent 5298047*. **1994**.
3. Blaszyk, P.E.; Christoff, W.R.; Gallagher, D.E.; Hawk, R.M.; Kiefer, W.J. Method and apparatus for introducing controlled spin in optical fibers, *U.S. Patent 6324872 B1*. **2001**.

4. Li, M.-J.; Chen, X.; Nolan, D.A. Fiber spinning for reducing polarization mode dispersion in single-mode fibers: theory and applications. *Proceedings of SPIE.* **2003**, *247*, 97–110.
5. DiGiovanni, D.J.; Golowich, S.E.; Jones, S.L.; Reed, W.A. Method of making an improved multimode optical fiber and fiber made by method. *Patent U.S. 2001/0019652.* **2001**.
6. DiGiovanny, D.J.; DiMarcello, F.V.; Jiang, X.L.; Oulundsen, G.E.; Pandit, S.P. Multimode optical fiber with increased bandwidth. *Patent U.S. 2004/0228590 A1*. **2004**.
7. Bohnert, K.; Gabus, P.; Kostovic, J.; Brandle, H. Optical fiber sensors for the electric power industry. *Opt. Lasers Eng.* **2005**, *43*, 511–526.
8. Kopp, V.I., Churikov, V.M., Singer, J., Neugroschl, D. Chiral fiber sensors. *Proceedings of SPIE* **2010**, *7677*, 76770U-1–76770U-6.
9. Kopp, V.I., Genack, A.Z. Adding twist. *Nature Photonics* **2011**, *5(8)*, 470–472.
10. Wong, G.K.L.; Beravat, R.; Russell, P.S.J. Helically twisted photonic crystal fibres. *Philos. Trans. R. Soc. A Math. Phys. Eng. Sci.* **2017**, *375*, 20150440.
11. Liu, T., Wang, D., Raenaei, R., Cheng, X., Zhang, L., Bennion, I. A low-cost multimode fiber Bragg grating sensor system, Proceedings of SPIE **2005**, *5634*, 54 – 61.
12. Sang, Xi., Yu, Ch., Yan B. Bragg gratings in multimode optical fibres and their applications. *Journal of Optoelectronics and Advanced Materials* **2006**, *8(5)*, 1616–1621.
13. Zhao, Ch.-L., Li, Zh. Demokan, M.S., Yang, X., Jin, W, Lu, Ch. Studies on strain and temperature characteristics of a slanted multimode fiber Bragg grating and its application in multiwavelength fiber Raman ring laser. *IEEE Journal of Lightwave Technology* **2006**, *24(6)*, 2394–2400.
14. Mizunami, T., Djambova, T.V., Niiho, Ts., Gupta, S. Bragg gratings in multimode and few-mode optical fibers, *IEEE Journal of Lightwave Technology* **2006**, *18(2)*, 230–235.
15. Yong, Zh., Zh., Ch., Yom, Sh. Multiple parameter vector bending and hightemperature sensors based on asymmetric multimode fiber Bragg gratings inscribed by an infrared femtosecond laser, *Optics Letters* **2006**, *31(12)*, 1794 – 1796.
16. An, J., Liu, T., Jin, Y. Fiber optic vibration sensor based on the tilted fiber Bragg grating, *Advances in Materials Science and Engineering* **2013**, *545013*, 1–4.
17. Li, D., Gong, Yu., Wu, Yu. Tilted fiber Bragg grating in graded-index multimode fiber and its sensing characteristics, *Photonic Sensors* **2013**, *3(2)*, 112–117.
18. Fang, Sh., Li, B., Song, D., Zhang, J., Sun, W., Yuan, L. A smart graded-index multimode fiber based sensor unit for multiparameter sensing applications, *Optics and Photonics Journal* **2013**, *3*, 265–267.
19. Guo, T., Guan, B.-O., Albert, J. Polarimetric multi-mode tilted fiber grating sensors, *Optics Express* **2014**, *22(6)*, 7330–7336.
20. Schmid, M.J., Muller, M.S. Measuring Bragg gratings in multimode optical fibers, *Optics Express* **2015**, 23(6), 8087–8094.
21. Gatchin, Yu.A., Demidov, V.V., Dukelskii, K.V., Ter-Nersesyants E.V. Quasi-single-mode fibers with an increased core size based on non-hexagonal microstructures. *Proceedings of Telecommunication Universities* **2017**, *3(3),* 37–42.
22. Demidov, V.V., Dukelskii, K.V., Leonov, S.O., Matrosova A.S. Nonlinear optical transformations of picosecond laser pulses in multimode microstructured fibers with moderate nonlinearity. *Proceedings of Telecommunication Universitie* **2018**, *4(1)*, 61–66.
23. Ananiev, V.A., Demidov, V.V., Leonov, S.O., Nikonorov, N.V. Hollow antiresonant fibers with a large effective area of the mode field for operation in the near and mid-IR spectral regions. *Proceedings of Telecommunication Universities* **2019**, *5(1)*, 6–14.
24. Agrawal G.P. *Nonlinear fiber optics*. Academic Press: Burlington, UK, 2012.
25. Olszewski, J., Szpulak, M., Urbanczyk, W. Effect of coupling between fundamental and cladding modes on bending losses in photonic crystal fibers. *Optics Express* **2005**, *13(16)*, 6015–6022.
26. Adams, M.J. *An Introduction to Optical Waveguides*; John Wiley & Sons Ltd.: New York, NY, USA, 1981.
27. Snyder, A.W., Love, J. *Optical Waveguide Theory*, Chapman & Hall: London, UK, 1983.
28. *Optical Fibres, Cables and Systems*, ITU-T Manual: Geneva, SW, 2009.
29. Guenther, B., Steel, D. *Encyclopedia of modern optics. Second edition. Volume 1.* Elsevier Science: Amsterdam, NL, 2018.
30. Bourdine, A.V., Barashkin, A.Yu., Burdin, V.A., Dashkov, M.V., Demidov, V.A., Dukelskii, K.V., Evtushenko, A.S., Ismail, Y., Khokhlov, A.V., Kuznetsov, A.A., Matrosova, A.S., Morozov, O.G., Pchelkin, G.A., Petruccione, F., Sakhabutdinov, A.Zh., Singh, G., Ter-Nersesyants, E.V., Tiwari, M., Zaitseva, E.S., Janyani, V., Yin, J. Twisted silica microstructured optical fiber with equiangular spiral six-ray geometry. *Fibers* **2021**, *9(27)*, fib9050027-1–fib9050027-17.
31. Bourdine, A.V. Modeling and simulation of piecewise regular multimode fiber links operating in a few-mode regime. *Advances in Optical Technologies* **2013**, *2013*, 469389-1–469389-18.
32. Bourdine, A.V., Delmukhametov, O.R. Calculation of transmission parameters of the launched higher-order modes based on the combination of a modified Gaussian approximation and a finite element method. *Telecommunications and Radio Engineering* **2013**, *72(2)*, 111–123.
33. Vasil'ev, S.A., Dianov, E.M., Medvedkov, O.I., Protopopov, V.N., Constantini, D.M., Iocco, A., Limberger, H.G., Salathe R.P. Properties of cladding modes excited in a fiber optical waveguide by refractive index gratings. *Quantum Electronics* **1999**, *26(1)*, 65– 68.